Dynamically Figured Kirkpatrick Baez X-Ray Micro-Focusing Optics

Peter J. Eng, Matthew Newville, Mark. L. Rivers, and Steve. R. Sutton

CARS, University of Chicago, Chicago, IL 60637

ABSTRACT

We present the optical designs, modeling, bender design and test results of x-ray micro-focusing optics used to micro-focus monochromatic undulator x-rays at the Advanced Photon Source (APS) The system uses two 100mm long, actively bent mirrors in a Kirkpatrick Baez arrangement. A detailed analytical model of the system's performance is described along with ray tracing results. A description of the integration of the benders into a complete micro-focusing system is provided. The system is easy to setup and use and is presently used in earth science research coupled to techniques such as micro-spectroscopy, fluorescence microprobe, and energy dispersive diffraction. The optics' performance is measured on the GeoSoilEnviroCARS microprobe experimental station at APS sector 13. Focusing tests using 10keV undulator x-rays resulted in a double focused beam with a horizontal and vertical full width at half maximum of 0.80μm x 0.85μm, and flux density gain greater than 10^5.

Keywords: micro-focusing, x-ray mirror, Kirkpatrick-Baez, micro-beam, microprobe, microspectroscopy

1. INTRODUCTION

High brilliance third generation synchrotron x-ray sources offer unprecedented opportunities for micro-beam optics development. The small size and divergence of these sources allow efficient use of a variety of traditional focusing concepts in the hard x-ray region. The Advanced Photon Source (APS) undulator at Argonne National Laboratory has a horizontal and vertical source size of 325μm x 43μm sigma and a horizontal and vertical divergence of 25μrad x 6μrad sigma. With such small divergence focusing optics can be placed 50m from the source and just in front (~.1m) of the sample. This results in demagnification ranging from 50 to 1000 with the optics intercepting as much as 5% of the total source.

The two successful micro-focusing optics presently being used at the APS are Fresnel zone plates[1, 2, 3] and Kirkpatrick-Baez[4, 5, 6, 7, 8] (KB) grazing incidence mirrors. There is a complementary relationship between these two optics. Zone plates are capable of producing focal spot sizes well below 1μm but must be refocused if the x-ray energy of interest falls outside the narrow band for a particular setting. KB mirrors are limited to focal spot sizes greater than 0.5μm but can deliver a significantly higher x-ray flux. KB mirrors are also achromatic, capable of focusing x-rays with an energy range wider than 50keV for a single setting of the optic.

At the Consortium of Advanced Radiation Sources (CARS), the Geology, Soil, and Environmental subgroup (GSECARS) is developing[9, 10, 11] Sector 13 at the APS. The optics for the sector are designed to accommodate the fact that many important Earth science samples are small, such as single crystals less than 10μm or aggregates with micron-sized structures and low elemental concentrations. To obtain a signal from these samples that will not be buried in background signal micron-sized focused beams are required. In most cases, the smallest useful spot size is 0.5μm, limited by lateral beam blurring due to finite sample thickness as well as the inability to keep a rotating single crystal centered to better than a few microns. Spectrally wide energy ranges are required for many of the measurement techniques used at GSECARS. Energy dispersive diffraction in diamond anvil cells (DAC)[10] avoids misalignment with respect to the incident beam by allowing the sample and detector to remain stationary. However, it requires x-ray energies ranging from 15-70keV in a single exposure. X-ray absorption fine structure (XAFS) measurements[11] often require monochromatic energy scans 1keV wide around multiple elemental edges up to 15keV apart. These spatial and spectral requirements along with the need for various working distances make dynamically figured KB mirrors the best choice to meet our scientific goals. In the remainder of this

Part of the SPIE Conference on X-Ray Microfocusing: Applications and Techniques
San Diego, California • July 1998
SPIE Vol. 3449 • 0277-786X/98/$10.00

paper we first present the modeling and design considerations used in developing our KB micro-focusing x-ray optics, followed by test measurements where we demonstrate sub-micron focal spots and achieve a flux density gain greater than 10^5.

2. OPTICAL DESIGN AND MODELING

In the KB optics arrangement two independent grazing incidence mirrors are arranged with their surface normal nearly perpendicular to the incident x-ray and rotated 90° relative to each other. Fig. 1 shows a schematic of this arrangement with the storage ring approximately 50m away and a 0.1m focal distance. The mirrors are set so that the central x-ray has a grazing incidence angle range from 1-5mrad corresponding to reflectivity cut off energies of 70-15keV for a mirror with a high density coating.

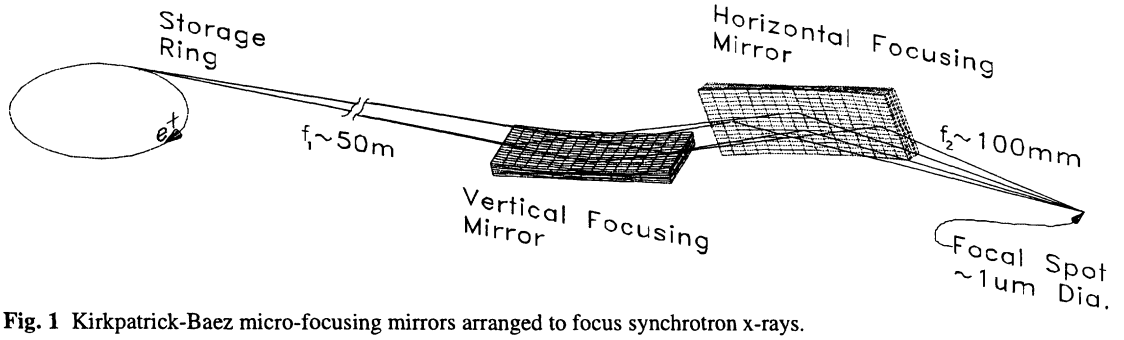

Fig. 1 Kirkpatrick-Baez micro-focusing mirrors arranged to focus synchrotron x-rays.

For the KB mirror system to form a demagnified image of the source without significant distortion, the mirror surface figure error must be smaller than the angular size of the source, given by:

$$S' = \frac{\sigma_s}{f_1} \tag{1}$$

where σ_s is the source size and f_1 is the distance of the optic to the source. If we describe all contributions to the mirror's slope error as σ_T' then the factor by which the focal image deviates from the ideal is given by:

$$D = \sqrt{\left(\frac{2\sigma_T'}{S'}\right)^2 + 1}\,. \tag{2}$$

The degree to which the optic preserves the source brilliance can be described as 1/D. The vertical angular source size S_V' of the APS undulator as viewed by a mirror 50m away is 0.9μrad ($S_H' = 6.5\mu rad$). To preserve 50% of the vertical brilliance, D must be less than 2 and the total RMS slope error budget of the vertical mirror (using eq. (2)) must be less than 0.8μrad. A RMS slope error this small represents the state of the art in the manufacture of flat mirrors and consumes nearly all the available slope error budget. This leaves little room for other sources of figure error such as the misfigure of the optical surface.

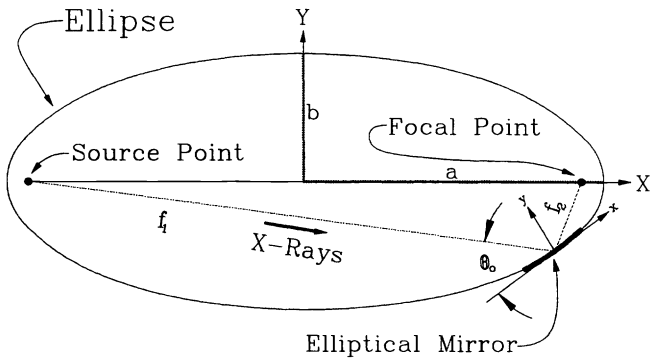

Fig. 2 The ideal mirror shape represented as a segment of an ellipse connecting the source point with the focal point.

The ideal mirror shape that will focus x-rays from the source point to the focal point is an ellipse with the source and focus located at the foci. Fig. 2 shows this arrangement with the mirror surface covering a small segment of the ellipse centered about the intersection of the x-rays and the ellipse. The equation of an ellipse in terms of its major and minor axes a and b is:

$$\frac{X^2}{a^2}+\frac{Y^2}{b^2}=1. \tag{3}$$

For the purpose of modeling optical performance it is convenient to transform[12, 9] to a mirror centered coordinate system with its origin at the mirror center and y-axis parallel to its surface normal. In this coordinate system, θ_o is the angle of incidence for the central ray, f_1 is the distance between the source point and mirror, and f_2 is the distance between the mirror and focal point. The ideal slope variation along the mirror's length is:

$$S(x)=2fK_o\left\{\left(2\nu\frac{x}{f'}+\mu\right)\left(1-\mu\frac{x}{f'}-\nu\frac{x^2}{f'^2}\right)^{-\frac{1}{2}}-\mu\right\} \tag{4}$$

where,

$$K_o=\frac{\tan\theta_o}{2f'},\qquad f'=\frac{f}{\cos\theta_o},\qquad f=\frac{f_1f_1}{f_1+f_2},$$

$$\mu=\frac{m-1}{m+1},\qquad \nu=\frac{m}{(m+1)^2},$$

and the demagnification is $m=\frac{f_1}{f_2}$.

Given the ideal slope function, a method of figuring the mirror surface to minimize the deviation from ideal was necessary. The sub-μrad total slope error required to preserve 50% of the brilliance requires that we use with the best flat mirror that could be manufactured and employ dynamic figuring through external bending forces.

To model the longitudinal figure of a beam with a moment of inertia $I(x)$, Young's modulas E and subject to a bending moment $M(x)$ we use the expression for the curvature of a beam:

$$K_M(x)=\frac{M(x)}{EI(x)}. \tag{5}$$

From Eq. (5) it can be seen that the figure of the beam can be made to vary along its length by adjusting the applied moment $M(x)$ and the shape through $I(x)$. To simplify the manufacturing of the mirror flat as well as reduce the chances that the mirror will "spring" when removed from the polishing jig we decided to maintain a constant thickness and only allow a linear change in the mirror width[12] resulting in a simple trapezoidal shape described as:

$$W(x)=W_o\left(1-\alpha\frac{x}{f'}\right), \tag{6}$$

where α is the taper factor. The moment of inertia for a beam of constant thickness t_o is, then

$$I(x)=I_o\left(1-\alpha\frac{x}{f'}\right), \tag{7}$$

where,

$$I_o=\frac{W_o t_o^{\,3}}{12}.$$

To allow for an asymmetric bending moment we use two adjustable bending forces on either end of the mirror resulting in a linear moment distribution:

$$M(x)=M_o\left(1+\eta\frac{x}{f'}\right), \tag{8}$$

where η is the asymmetry factor for the moment distribution. Eq. (5) now can be written as:

$$K_M(x) = K_o\left(1+\eta\frac{x}{f'}\right)\left(1-\alpha\frac{x}{f'}\right)^{-1}, \tag{9}$$

where $K_o = \frac{M_o}{EI_o}$ is equal to the inverse of the central radius of curvature. Since it is the slope error that needs to be minimized we integrate Eq. (9) arriving at the expression for the slope of the bent mirror along its length:

$$S_M(x) = -\frac{K_o f'}{\alpha^2}\left\{\eta\alpha\frac{x}{f'} + (\eta+\alpha)\ln\left(1-\alpha\frac{x}{f'}\right)\right\}. \tag{10}$$

In Eq. (10) f' describes the geometry of the mirror setup whereas K_o, η and α are determined by performing a non-linear least squares fit of Eq. (10) to Eq. (4) with constant weighting. After determining the curvature, taper and moment distribution that minimizes the slope error, the RMS slope error due to mirror misfiguring can be calculated using:

$$\sigma'_M = \sqrt{\left[\int_{-L/2}^{L/2}\left(S(x)-S_M(x)\right)^2 dx\right]}. \tag{11}$$

To determine the total RMS slope error we add in quadrature to Eq. (11) the static RMS slope error of the flat mirror σ'_F yielding:

$$\sigma'_T = \sqrt{{\sigma'_M}^2 + {\sigma'_F}^2}. \tag{12}$$

Substituting Eq. (12) into Eq. (2) we can estimate the full width at half maximum (FWHM) of the focal spot as:

$$FWHM = 2.35D\sigma_s m. \tag{13}$$

To aid in achieving our goal of a 1μm FWHM focal spot we use this analytical model to guide our design efforts. An important constraint on the system's design is the requirement that the working distance be sufficient to allow enough space for the sample, detector and other instrumentation (in our case an optical microscope.) For our setup, a 20mm gap from the end of the horizontal mirror and the focal spot is sufficient. Using a 100mm long mirror results in a distance from the mirror center to the focal spot f_2^H of 70mm. At 55mm from the source this arrangement achieves a demagnification of 787, sufficient to reach our 1μm goal. With a 100mm vertical mirror immediately upstream $f_2^V = 170mm$ results in a demagnification of 323, also adequate to achieve 1μm assuming aberrations are kept small.

Table 1 Mirror Geometry

	Vertical Mirror	Horizontal Mirror
f_1	55m	55.1m
f_2	0.170m	0.070m
m	323	787

The APS undulator source is very astigmatic with a FWHM of 763μm horizontal and 101μm vertical. It is therefore advantageous to place the horizontal mirror closest to the sample, resulting in a greater demagnification. Performing the above analysis with perfectly flat KB mirrors 100mm in length set to an incidence angle of 5mrad with the geometry in Table 1 we determined that the $FWHM_H$ = 1.0μm and $FWHM_V$= 0.32μm, nearly ideal. Fig. 3 shows a plot of the slope error for both vertical (solid lines) and horizontal (dashed line) mirrors. From Fig. 3 we see the RMS slope error is much larger in the horizontal than the vertical (0.74μrad vs. 0.02μrad) but both are small when compared to their respective angular source sizes (5.9μrad vs. 0.78μrad).

This analytical approach to evaluating the performance of tapered KB mirror optics is extremely useful since calculations run almost instantly allowing the testing of many different configurations. As a check on this analytical approach, we developed a ray tracing program that is optimized for the KB mirror geometry. Fig. 4 shows the results of tracing 150,000 rays using the configuration above. The FWHM determined from the horizontal and vertical histograms are 1.2μm x 0.40μm and agree well with the values determined from the analytical calculations, confirming the validity of the method.

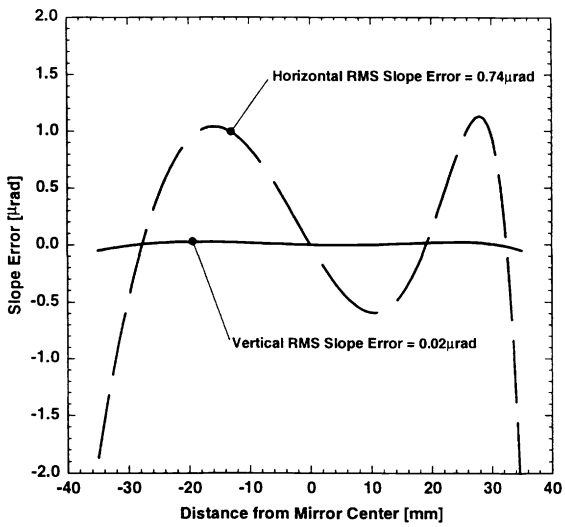

Fig. 3 Deviation of vertical (solid line) and horizontal (dashed line) mirror slope from that of an ideal ellipse. Calculated using the APS undulator source $FWHM_H = 763\mu m$, and $FWHM_V = 101\mu m$ and mirrors set to the values in Table 1 achieving a focal spot of $FWHM_H = 1.0\mu m$, $FWHM_V = 0.32\mu m$.

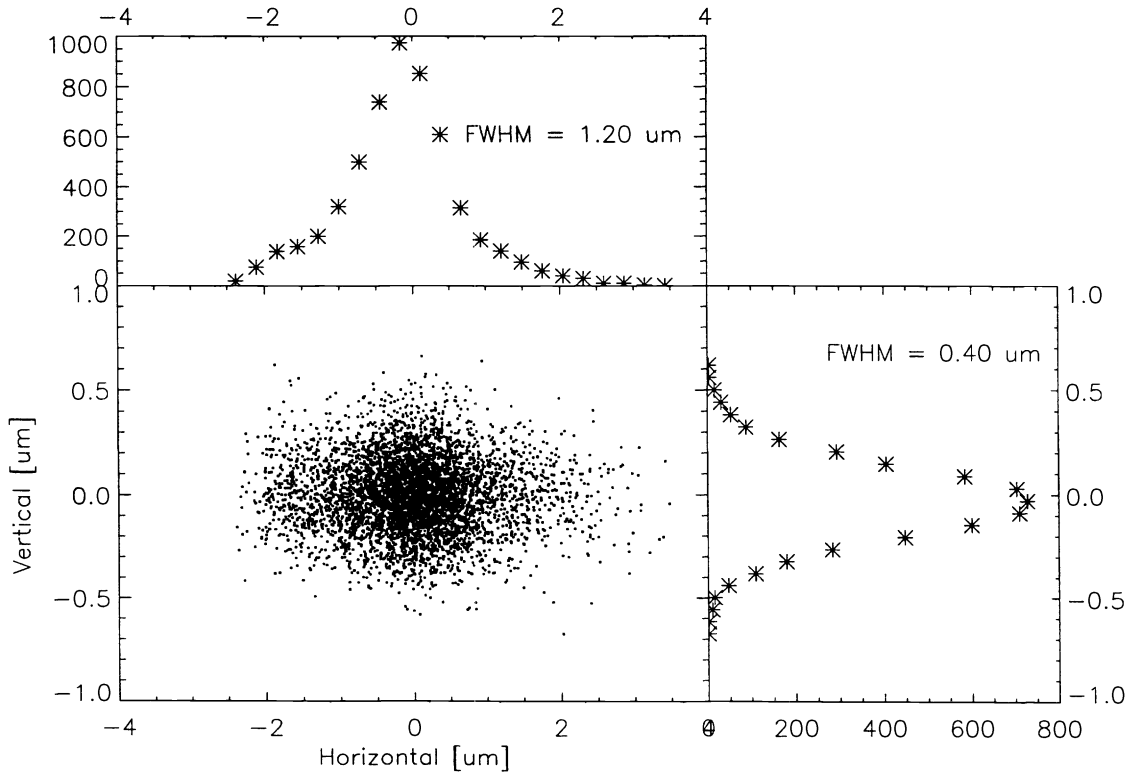

Fig. 4 Ray trace of the KB mirrors figured as shown in Fig. 3 using the mirror geometry of Table 1. The APS source size and divergence was modeled using a Gaussian distribution of 150,000 rays with $\sigma_V = 43\mu m$, $\sigma_H = 325\mu m$, $\sigma'_V = 6\mu rad$ and $\sigma'_H = 25\mu rad$.

Using the mirror geometry in Table 1 we modeled the performance of the system operating at 1, 3 and 5mrad. Table 2 shows a summary of the results for the vertical and horizontal mirrors. In the table the

Table 2 Results of Micro-Focusing Model Analysis

Vertical Mirror
Ideal = 0.32μm, f_1 = 55m, f_2 = 170mm

Mirror Setting		Fit Results			Incidence θ_o Variation			Calculated Performance				
								Perfect Flat			1μrad Flat	
θ_o [mrad]	Aperture [μm]	1/Ko [m]	η	α	ΔSlope [mrad]	ΔEc [keV]	Ec [keV]	σ'm [μrad]	FWHM [μm]	Gain	FWHM [μm]	Gain
1	70	339	0.25	1.24	0.21	15	70	0.004	0.32	219	0.86	81
3	210	113	0.25	1.24	0.64	5	23	0.011	0.32	656	0.86	244
5	350	68	0.25	1.24	1.10	3	14	0.018	0.32	1094	0.86	407

Horizontal Mirror
Ideal = 0.97μm, f_1 = 55.1m, f_2 = 70mm

Mirror Setting		Fit Results			Incidence θ_o Variation			Calculated Performance				
								Perfect Flat			2μrad Flat	
θ_o [mrad]	Aperture [μm]	1/Ko [m]	η	α	ΔSlope [mrad]	ΔEc [keV]	Ec [keV]	σ'm [μrad]	FWHM [μm]	Gain	FWHM [μm]	Gain
1	70	140	0.29	1.20	0.6	36	70	0.150	0.98	71	1.2	58
3	210	46	0.29	1.20	1.8	12	23	0.450	0.99	212	1.2	175
5	350	28	0.29	1.20	3.0	7	14	0.740	1.00	350	1.2	292

"Aperture" is simply the 70mm long optical surface of the mirror multiplied by the incidence angle, and the gain is the ratio of the "Aperture" to the "FWHM" assuming 100% reflectivity (actual reflectivity is closer to 80%.) Under "Fit Results" it is interesting to note that η and α are constant for each mirror even though they were free to vary during the fit, with only the central radius of curvature $1/K_o$ varying. From Table 2 it can be seen that for these highly curved optics there is a large variation in the incidence angle resulting in a ±11% variation in the critical energy E_c. Under "Calculated Performance" we can see that the RMS slope error σ'_m increases with increasing θ_o due to the increases in ellipticity. For both the vertical and horizontal mirror in the case of a perfect flat the focal size is nearly ideal and in both cases it is the addition of RMS slope error to the mirror figure that dominates the aberration, underscoring the importance of acquiring high quality mirrors.

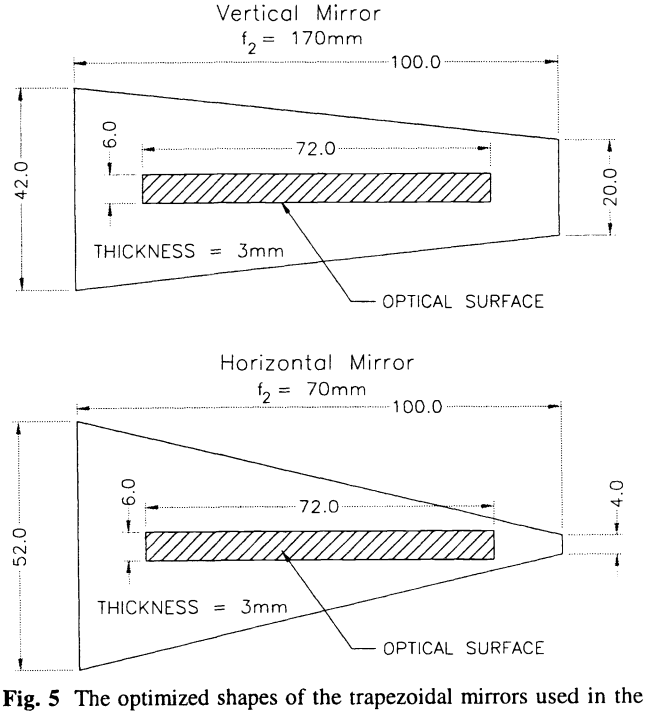

Fig. 5 The optimized shapes of the trapezoidal mirrors used in the micro-focusing tests.

The taper factor α for each mirror is determined from the fits. Using Eq. (6) and the value for α and f_2 from Table 2 we can determine the width profile for each mirror. Fig. 5 shows the shapes of the trapezoidal mirrors we used in the test results to follow. The mirror blanks were cut from a 5" diameter single crystal Si boule at the APS optical fabrication lab. Final grinding and polishing was performed by Continental Optics, Inc[13]., where an RMS slope error of 1μrad and surface roughening of 2Å was achieved. The mirrors were then coated at the APS deposition laboratory first with a binding layer of 50Å Cr and then 400Å Rh.

3. MIRROR BENDER DESIGN

With the KB arrangement and the mirror shape and specification defined, we can now consider the mirror bender design and operation. The ability to dynamically figure the mirror while monitoring the focal spot is essential for producing the best optical focus and improving ease of use. On-line adjustability of the figure allows the user to change the mirrors' cut-off energy and working distance to best match the experiment. On the other hand, a bender with too many adjustable parameters is difficult to optimize. It is also important that the adjustments have low hysteresis, fine enough resolution and not drift over time. We have developed a two parameter bender that meets all of these requirements.

The ends of the mirror are supported from below by two fixed rods. Above the surface and inboard from the fixed rods are two bending rods through which the bending forces are applied. The expression for the upstream F_1 and downstream F_2 forces are:

$$F_1 = \frac{M_o}{r}\left[1 - \frac{\eta(L+2r)}{2f_2}\right] \tag{14}$$

$$F_2 = \frac{M_o}{r}\left[1 + \frac{\eta(L+2r)}{2f_2}\right] \tag{15}$$

where, $M_o = K_o E I_o$, E is Young's modulus, L is the distance between the two inner bending rods and r is the distance between the inner and outer rods -- the level arm used in producing the moments applied to either end of the mirror. The bending forces F_1 and F_2 for the mirrors shown in Fig. 5 and with the bender set to the values in Table 2 are less than 10 lbs. It is very important that the bender be designed to apply only pure moments and operate without sticktion. The detailed bender design used is described in our early paper[7]. Here we will describe our latest integration of our bender into a complete micro-focusing system.

Fig. 6 shows the GSECARS KB micro-focusing system. The top panel shows the horizontal and vertical benders mounted on a common mounting bar, allowing the beam apertures of both benders to precisely align. The two benders are identical, each having four actuators, two for the bending forces, one to adjust the incident angle, and one to adjust the position of the mirror in the direction of its surface normal. The actuator for the incidence angle has a range of ±20mrad and functions by rotating the mirror assembly on an axis aligned with the mirror surface through flex pivots, actuated by a drive cam. The eight drive motors are identical low current bipolar miniature stepping motors that are powered by an inexpensive eight axis driver. The bender mounting bar is universal and allows the benders to be configured to "bounce" the x-rays to the left or right, and up or down. The lower panel of Fig. 6 shows a photo of the system installed on the undulator microprobe table at GSECARS APS sector 13. It is on this table, 55m from the source, that we performed the micro-focusing measurements described in the next section.

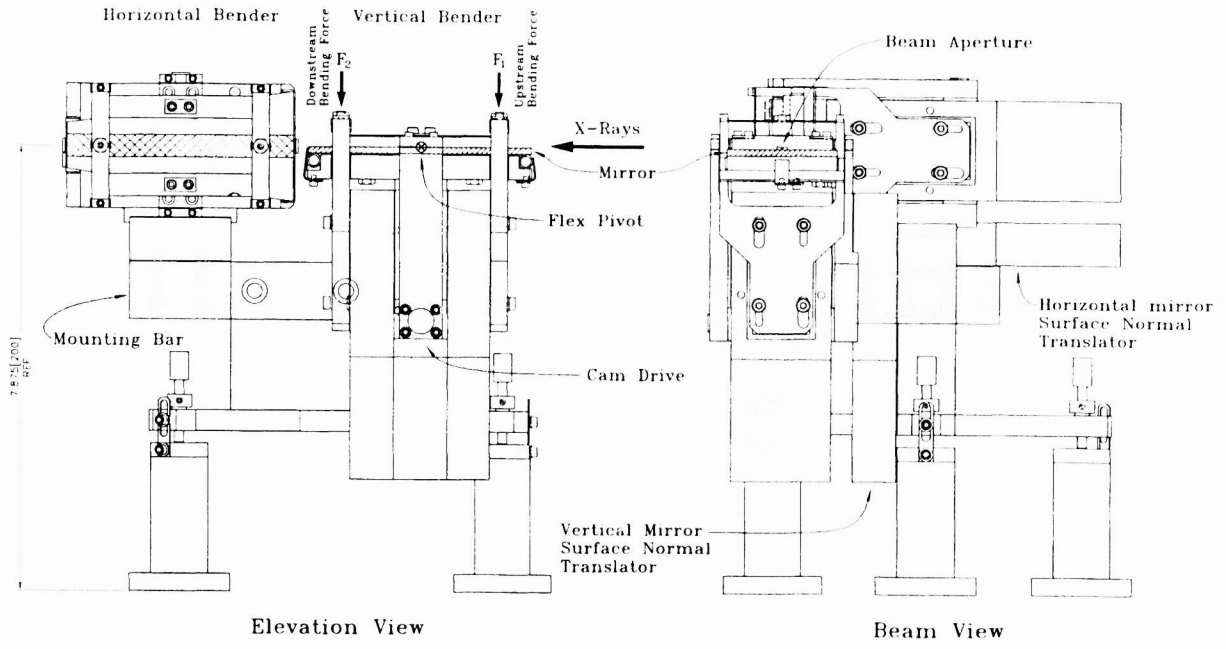

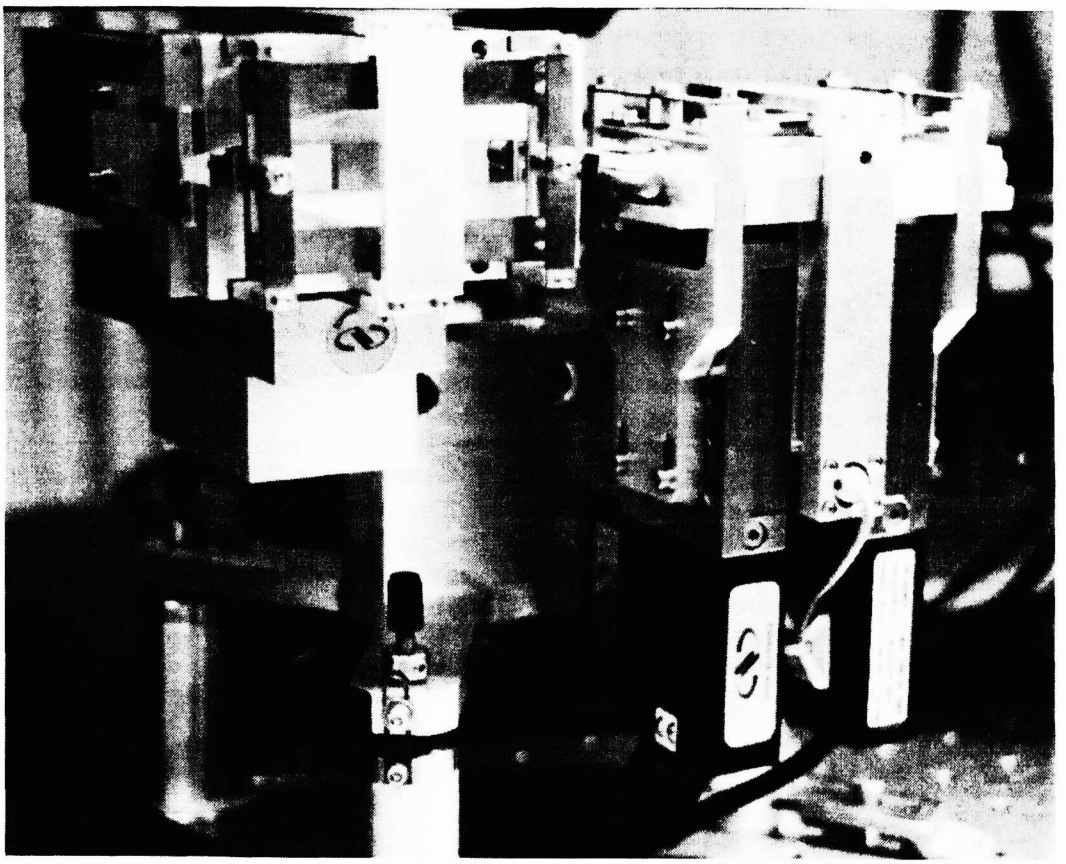

Fig. 6 GSECARS KB micro-focusing system. The top panel shows the horizontal and vertical benders mounted on a common mounting bar with their beam apertures aligned. The lower panel shows a photo of the system installed on the microprobe table (beam enters from the right.)

4. MICRO-FOCUSING TEST RESULTS

The integration of micro-focusing beam diagnostics into our x-ray microprobe instrument is essential to exploit the flexibility of the dynamic KB system. At the start of each experiment the focal spot is located and optimized allowing the sample position to be scanned in the focal plane.

Fig. 7 shows a schematic of the x-ray[14, 11] microprobe/micro-focusing test setup. Monochromatic or "white" x-rays enter from the left passing through a pair of adjustable horizontal and vertical slits. The slits are used to locate the x-ray "foot print" on the correctly figured mirrors' central 70mm (the distance between the two inner bending bars). They are then reflected from the mirror and focused on the sample location where the sample is supported by a 0.1μm resolution XYZ scanning stage.

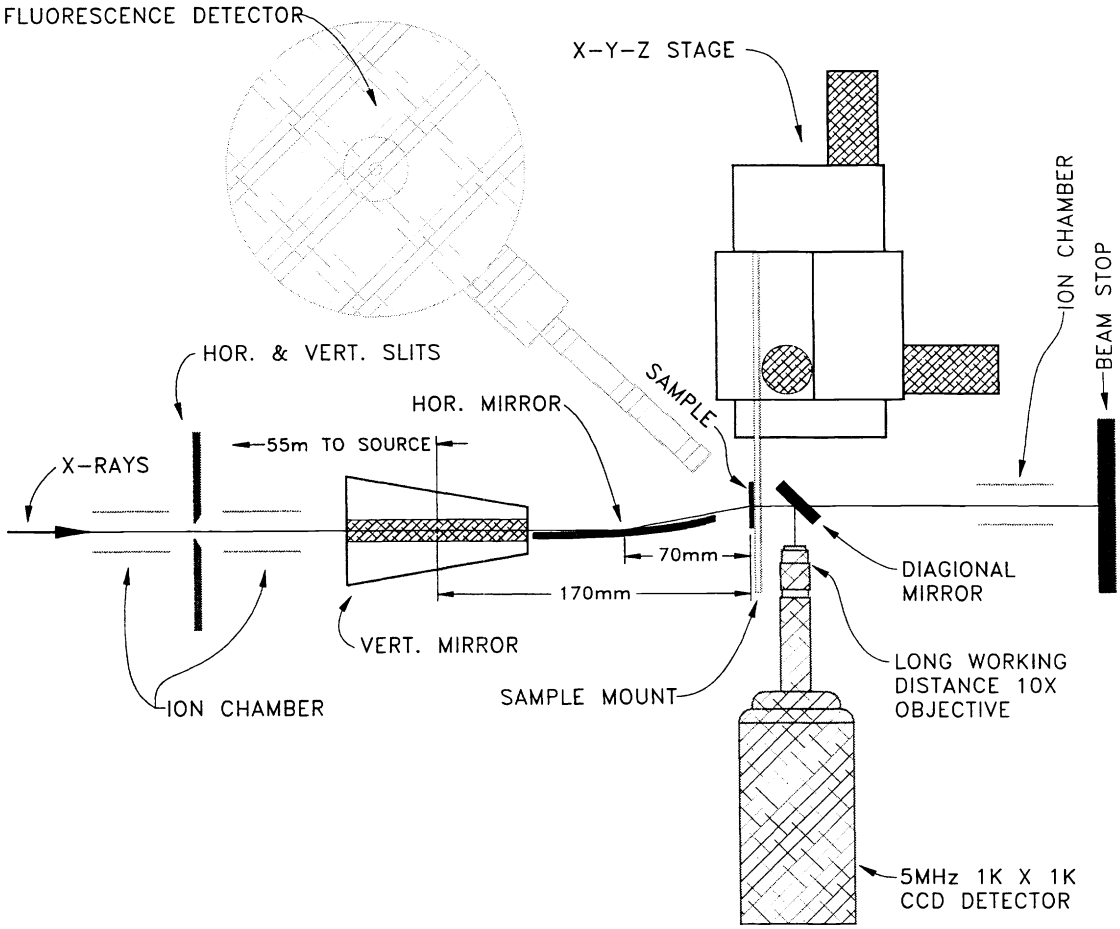

Fig. 7 Schematic of the x-ray microprobe / micro-focusing test setup.

For our test measurements three different "samples" and detector combinations were used. The most valuable, allowing rapid optimization of the focus, is the fluorescence screen visible light microscope combination. In this setup a 0.5mm thick transparent YAG:Ce crystal[15] produces visible light ($\lambda = 55$nm) over only a 5μm thick (Ce doped) optically active layer. This is reflected from a diagonal mirror into a Mitutoyo, 10X, long working distance (32mm) objective (NA = 0.28). The objective produces a magnified image on a cooled (-35°C) 9x7mm Kodak 1317 x 1035 (6.7μm pixel size) CCD. The CCD is read by a 12 bit, 5 MHz, Princeton Instruments Inc. "Pentamax" camera and controller. This system allows us to rapidly display (3Hz) high resolution focal spot images on the computer screen where the vertical and horizontal cross-section can be measured and optimized for maximal sharpness, in real time, by adjusting

the bending forces. The system resolution is about 3μm, sufficient to allow us to visibly "tweak" up the horizontal and vertical focus to nearly their optimal settings in just a few minutes.

Our second sample detector combination is used to make quantitative measurements of the focal size as well as further optimize the mirror bender settings. The method used is often referred to as a fluorescence knife edge. It works by monitoring Ni and Cr fluorescence with a solid state detector as the edge of a 0.5mm Si wafer coated with 1000Å of each is scanned through the beam. The edge is formed by breaking the wafer at LN_2 temperature so that the metal coating is brittle and forms a sharp, thin film edge[16]. The resolution of this system is better than 0.1μm and produces enough fluorescence signal to allow fast scanning (< 0.1sec/point.)

Our third combination is used to measure the system's reflectivity efficiency. In this case a pure SiO_2 glass screen is placed at the sample position and the energy spectrum of the scattered radiation is measured with the solid state detector. The ratio of the reflected to directly scattered energy spectrum determines the reflectivity as a function of energy.

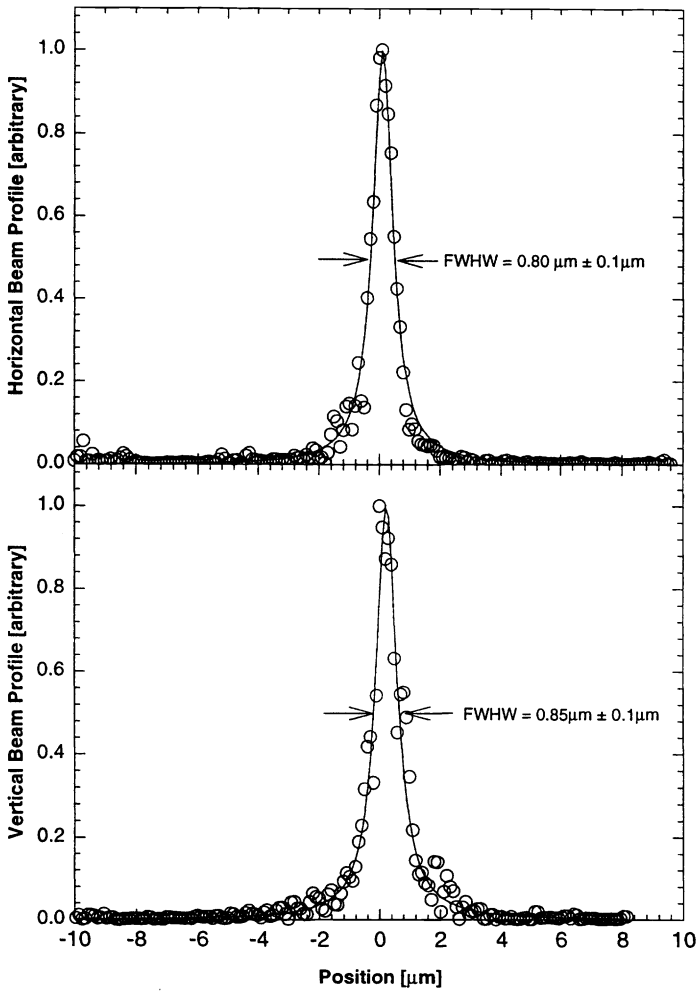

Fig. 8 Double focused 10keV undulator beam. The entrance aperture of both mirrors is 350μm. With a 63% reflectivity the flux density in this focal spot is 10^5 greater than the un-focused beam.

We conducted our micro-focusing test using monochromatic x-rays from a water-cooled channel cut <220> Si monochromator tuned to the undulator first harmonic set at 10keV. The KB optics were arranged as described in Table 2. The mirrors were illuminated with a 350 x 350μm beam, and both mirrors were set to 5mrad. The focus was optimized visually first, using a fluorescence screen and microscope and then by performing horizontal and vertical edge scans. The visual optimization brings us very close to the best focus, with only small changes made to the bending forces after the edge scans.

Fig. 8 shows our optimized double focused beam. The derivative of the edge scans are plotted and the solid lines are Lorenzian fits. The horizontal FWHM is 0.80μm ± 0.1μm, showing perfect focusing. The vertical FWHM is 0.85μm ± 0.1μm a factor of 2.8 larger than ideal but consistent with the value predicted by Eq. 2, given the 1.0μrad RMS slope error σ'_F of the mirror and a 0.8μrad angular source size S'_V. In the vertical direction it is interesting to note that the focal size could be cut nearly in half (assuming the focus is limited by the quality of the mirror,) if a 0.5μrad mirror could be fabricated.

Wide scans, ± 50μm, were performed to obtain a measure of the intensity found in the wings. From the integrated intensity of these edge scans it was found that compared to a central 8μm wide region the percentage of the beam found in a combined 40μm region on both sides of the central region was 6.5% for horizontal edge scans and 4.8% for vertical scans. We also monitored the stability of the focus and found that over a period of eight hours there was no significant change in the beam size or position.

Table 3 shows the results of the reflectivity measurements for focused 10keV x-rays and $\theta_o = 5mrad$. The values are shown for each mirror inserted individually and inserted together. The critical energy at this angle for both Rh coated mirrors is 14keV. The horizontal reflectivity is lower due to the wider range of incident angles along its length, rounding the reflectivity curve, and reducing some of the intensity at 10keV (see Table 2.)

Table 3 Mirror Reflectivity

Horizontal	Vertical	Both
73%	87%	63%

The flux density gain of the system is the ratio of the area of the entrance aperture to the area of the focal spot multiplied by the percent reflectivity. Using the value from Table 3 of 63% and the FWHM from Fig. 8 the flux density gain for the sub-micron double focused beam is 1.1×10^5 with the optics collecting approximately 4% of total first harmonic flux that is passed by the Si monochromator.

5. CONCLUSION

We have demonstrated that the performance of our dynamically figured KB micro-focusing optics has met our theoretical predictions. A 0.80x 0.85μm FWHM focused beam has been achieved with a gain greater than 10^5. The analytical model developed for simulating the system's performance has allowed us to optimize the trapezoidal mirror shape, determine the specifications for substrate quality, and design a mechanical bender capable of accurately figuring the mirrors' surface.

In the future we plan on continuing our focusing tests of both undulators monochromatic beam and full "white" spectrum as well as the APS bending magnet (monochromatic and white) beam. Additional tests will be performed on focal stability during energy scans where both the undulator gap and the monochromator angle are changed at the same time. We will enclose the bender in a He box to reduce absorption by air and protect the mirror surface from chemical attack. The effects of full undulator beam at closed gap will be determined, regarding both the thermal distortion of these un-cooled mirrors, and damage to the mirror substrate and coating. We will continue testing mirror substrate alternatives to Si, with high purity SiO_2 glass showing promising initial results. We also will be working with mirror manufacturers in an attempt to develop a procedure for fabricating vertical focusing mirrors with RMS slope errors 0.5μrad or less.

6. ACKNOWLEDGMENTS

This work is supported by the NSF - Earth Sciences EAR-9317772 and EAR 92-14163, DOE - Geosciences DE-FGO2-94ER14466 and DE-FGO2-96ER14648 and W. M. Keck Foundation. We gratefully acknowledge the assistance: by Nicholas Molders in mirror characterization and building the motor control electronics, Chian Liu from the APS Deposition Laboratory for coating the mirrors, Ruben Khachatryan and Szczesny Krasnicki from the APS optical fabrication Laboratory for grinding and etching the Si mirror blanks, Wenbing Yun for providing the fluorescence knife edge, Fred Sopron and Mike Jagger for technical assistance in building the micro-focusing system and Wilfried Schildkamp and Mati Meron for helpful discussions on the subject.

7. REFERENCES

[1] B. Lai, W. Yun, Y. Xiao, L. Yang, D. Legnini, Z. Cai, A. Krasnoperova, F. Cerrina, E. DiFabrizio, L. Grella and M. Gentili, Rev. Sci Instrum. **66**, 2287 (1995)
[2] E. DiFabrizio, M. Gentili, L. Grella, M. Baciocchi, A. Krasnoperova, F. Cerrina, W. Yun, B. Lai and E. Gluskin, J. Vac. Sci. Tec. B **12**, 3979 (1994)
[3] Z. Chen, Y. Vladimirsky, M. Brown, Q. Leonard, O. Vladimirsky, F. Moore, F. Cerrina, B. Lai, W. Yun and E. Gluskin, J. Vac. Sci. Tec. B **15**, 2522 (1997)
[4] P. Kirkpatrick and A. V. Baez, J. Opt. Soc. Am. **38,** 766 (1948).
[5] J. H. Underwood and D. Turner, Proc. **SPIE 106**, 125 (1977).
[6] A. C. Thompson, K. L. Chapman, G. E. Ice, C. J. Sparks, W. Yun, B. Lai, D. Leginni, P. J. Viccaro, M. L. Rivers, D. H. Bilderback, and D. J. Thiel, Nucl. Instrum. Methods A **319**, 320 (1992).
[7] P. J. Eng, M. Rivers, M. B. X. Yang and W. Schildkamp, In X-ray microbeam technology and applications, W. Yun, ed., Proc. **2516**, 41 (1995)
[8] B. X. Yang, M. L. Rivers, W. Schildkamp, and P. J. Eng, Rev. Sci. Instrum. **66 (2)**, 2278 (1995).
[9] Y. Wang, M. Rivers, S. Sutton, P. J. Eng and G. Shen, Proceedings of AIRAPT and High-Pressure Conference of Japan, in press, (1998)
[10] T. S. Duffy, G. Shen, M. Rivers, S. Sutton, P. J. Eng, Y. Wang, D. Heinz, H. K. Mao, R. J. Hemley, Y. Ma and J. Hu, Eos, Transactions, Am. Geophys. Union, **78**, S313 (1997)
[11] S. R. Sutton, M. L. Rivers, P. J. Eng, and M. Newville, Eos Trans. Amer. Geophys. Union, **78**, F789, (1997)
[12] B. X. Yang, Appl. Opt. (submitted).
[13] P. Z. Takacs, S. F. Feng, E. L. Church, S. Qian, and W. Liu, Proc **SPIE 966**, 364 (1988).
[14] M. L. Rivers, S.R. Sutton, and K. W. Jones, Synchrotron Radiat. News **2**, 23 (1991).
[15] A. Koch, C. Raven, P. Spanne and A. Snigirev, J. Opt. Soc. Am. A **15**, 1940 (1998)
[16] Fluorescence edge kindly supplied by WenBin Yun.